Automatic Segmentation of Blood Vessels from Dynamic MRI Datasets

Olga Kubassova

School of Computing, University of Leeds, UK
olga@comp.leeds.ac.uk*

Abstract. In this paper we present an approach for blood vessel segmentation from dynamic contrast-enhanced MRI datasets of the hand joints acquired from patients with active rheumatoid arthritis. Exclusion of the blood vessels is needed for accurate visualisation of the activation events and objective evaluation of the degree of inflammation. The segmentation technique is based on statistical modelling motivated by the physiological properties of the individual tissues, such as speed of uptake and concentration of the contrast agent; it incorporates Markov random field probabilistic framework and principal component analysis. The algorithm was tested on 60 temporal slices and has shown promising results.

1 Introduction

In Dynamic Contrast-Enhanced Magnetic Resonance Imaging (DCE-MRI) sequences of images are acquired over time, during which a contrast agent (normally gadolinium diethylene triamine pentacetic acid (Gd-DTPA)) pre-injected into the patient enhances disease affected tissues [1]. Measurement of this enhancement, which is specific for voxels representing particular tissue types, allows assessment of the patient's condition [2,3].

The enhancement is reflected by the shape of signal intensity vs. time curves derived on the voxel-by-voxel basis from the temporal slices and can be measured by computing various heuristics such as maximum rate of enhancement (ME), initial rate of enhancement (IRE), and time of onset of enhancement (T_{onset}) [4,3,5]. Positioning of the imaging volume for acquisition of the data from the 2nd–5th metacarpophalangeal joints (MCPJs) and structure of the DCE-MRI experiment are shown in Fig. 1.

It was demonstrated [6] that signal intensity vs. time curves normalised over a baseline ($\hat{I}$) can be classified into one of the four categories based on their pattern of contrast agent uptake. The heuristics therefore can be extracted from these approximations rather than the raw data (Fig. 2), making their estimation more

* We gratefully acknowledge the advice and support of Dr. A. Radjenovic, Dr. S. F. Tanner [Medical Physics, University of Leeds] and Prof. R. D. Boyle, Dr. M. Everingham [School of Computing, University of Leeds]. Dr. Tanner is further thanked for providing medical data. O. Kubassova acknowledges with thanks the UK Research Councils for financial support via a Dorothy Hodgkin Award.

N. Ayache, S. Ourselin, A. Maeder (Eds.): MICCAI 2007, Part I, LNCS 4791, pp. 593–600, 2007.
© Springer-Verlag Berlin Heidelberg 2007

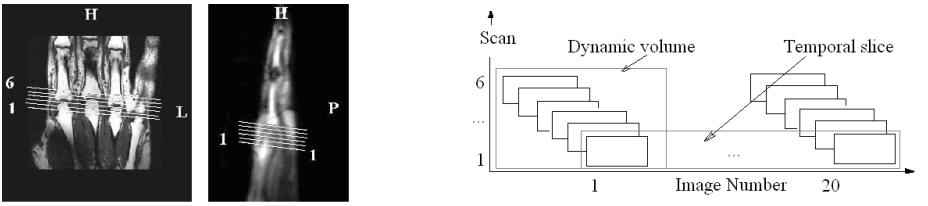

Fig. 1. Left: Positioning of imaging volume. Right: Structure of 4D DCE-MRI dataset with 6 temporal slices, 20 dynamic volumes.

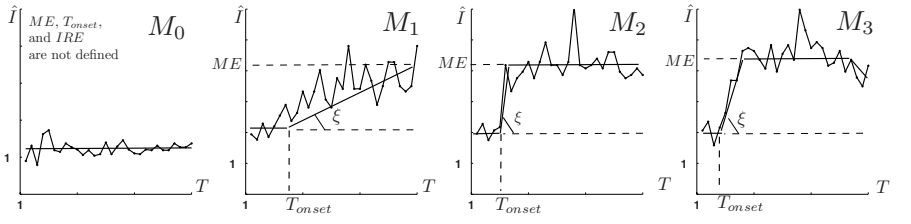

Fig. 2. Signal intensity vs. time curves normalised over a baseline ($\hat{I}$) approximated by M_0–M_3; ξ is a slope of the $\hat{I}$ that be taken as IRE; ME has not been reached for model M_1

robust to the noise effects and subjective opinion of the operator. Classification of $\hat{I}$ is based on the shape of the curve and the noise distribution presented in the temporal slice. The categories are:

M_0 – negligible enhancement, corresponding to the tissue allocated within cortical and trabecular bone, inactive joints, skin and disease unaffected areas.
M_1 – base/wash-in, corresponding to the curves in which by the end of the scanning procedure the maximal intensity has not been reached, indicating constant leakage into locally available extra-cellular space.
M_2 – base/wash-in/plateau. Full absorption of the contrast agent by the tissues.
M_3 – base/wash-in/plateau/wash-out. The wash-out phase is observed at the end of the scanning procedure.

To quantify the degree of RA, radiologists measure a number of voxels within a certain range of the heuristics ME and IRE. Due to the high vascularity that occurs in disease affected tissues, behaviour of the blood vessels and such tissues will be depicted in a very similar manner. This complicates visual analysis of the data and does not permit an objective assessment of the inflammation.

2 Related Work

A number of blood vessel segmentation techniques have been proposed [7,8,9]. Algorithms for static MRI and computer tomography (CT) data segmentation

[10,11] attempt to estimate the centre of the vessel paths and then employ various tracking techniques or prior knowledge about the imagery to determine vessel tree structure. In [7,12] explicit models (deformable models, parametric models, and template matching) were applied to extract the vasculature from DCE-MRI datasets. Such methods generally require manual or semi-automatic initialisation based on prior information about the diameter and location of the vessels.

Classification based methods are also popular for vessel segmentation from DCE-MRI data. Early methods [13] were based on the assumption that each voxel that enhances more than a certain threshold is vascular in origin. However, this approach can lead to the exclusion of up to 50% of the voxels from the image in enhancing tumours and other vascular tissues [5].

These methods have been enhanced by various modelling techniques. The Expectation Maximisation (EM) algorithm is widely used for tissues classification [14]. Commonly, classification is done based on intensity values [15] and whilst performance of these techniques is promising, intensity values of the tissues do not provide enough information for the data classification and the majority of the techniques require some post-processing in order to eliminate falsely detected regions.

We propose to perform blood vessel segmentation using heuristics ME, IRE, and a model number M as classification attributes rather than intensity values. These parameters utilise information about the tissues and should describe behaviour of the voxels better.

3 Segmentation Algorithm

Tissues with the most active perfusion and blood vessels normally exhibit a wash-out phase and assume model M_3, the rest of the disease-affected tissue is normally approximated with M_2, which indicates presence of the intensity plateau in $\hat{I}$ [6]. To isolate and locate tissues with the most significant temporal course variations we applied principal component analysis (PCA) to the temporal slices, where voxels, whose $\hat{I}$ curves were approximated by M_0 and M_1 were excluded.

Our experiments show that the first two principal components capture 97% of the variance in the data. It has also been illustrated that in DCE-MRI studies of the MCPJs, the first component shows temporal course compatible with inflammatory enhancement and the second – with blood vessels and areas with the most active perfusion [16]. Variation of the first two components around the mean and the projection of the data to the first and second components are shown in Fig. 3.

Global thresholding of the images, obtained as a projection of the original data to the second principal component with iterative thresholding [17] allows exclusion of the voxels with insignificant enhancement. Having excluded these, the task is to assign labels {vessel / non-vessel} to the remaining voxels.

Empirically it was observed that the distribution of the heuristics ME, IRE, and a model number M on the remaining voxels is bimodal, the heuristics exhibit

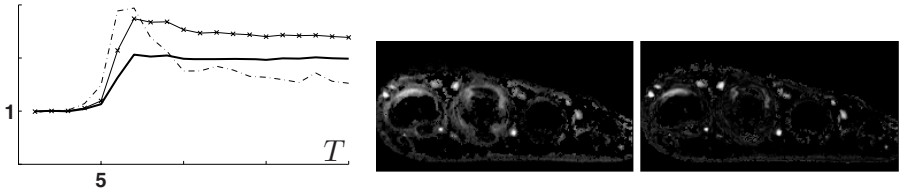

Fig. 3. From the feft: For a temporal slice: mean (bold), mean+2 first principal component(−×−), and mean+2 second principal component $(- \cdot -)$; projection of the data on the first (middle) and second (right) princupal component

higher values on voxels corresponding to the vessels. We fit the mixture model of two Gaussians to the data using EM algorithm and assign a label {vessel / non-vessel} based on the assumption that the cluster with the higher mean corresponds to the vessel.

Let N be the number of voxels $\{x_i\}_{i=1...N}$ in the slice, each voxel characterised by three parameters $\mathbf{x} =< ME, IRE, M >$. Let $\mathbf{\Theta}$ denotes the mixture parameters (the mean and standard deviation), and $l = \{l_1, l_2\}$ is vessel / non-vessel class, then:

$$p(\mathbf{x}|\mathbf{\Theta}) = \sum_l p(\mathbf{x}|l, \mathbf{\Theta})\pi_l(l), \tag{1}$$

where π_l represents proportion of each class within the data and $p(\mathbf{x}|l, \mathbf{\Theta})$ – probability of a voxel to belong to the class l_1/l_2. We label each voxel with l_1/l_2, so that it gives the greater likelihood:

$$\Theta^*(\mathbf{x}) = \quad \mathtt{arg}\max_{\mathbf{\Theta}} \sum_{i=1}^{N} \log p(x_i|\mathbf{\Theta}) \tag{2}$$

However, the noise presented in the data and imprecision in the model we used leave some error (see Fig. 5). Therefore, we exploit the fact that blood vessels have nonnegligible spatial support by assuming that neighbouring voxels are likely to have the same label in the absence of significant differences in the grey level between them.

Markov random field (MRF) [18] based filtering allows refining our initial labelling. Let Λ be a field of labels over the image, and C – a set of clicks, defined in 8-connected neighbourhood [19], then the energy function can be described by Eq. 3, where we omitted dependence on fixed parameters $\mathbf{x}$ and $\mathbf{\Theta}$ for the sake of clarity.

$$E = \sum_{i=1}^{N} \log p(x_i|l_i) + \lambda \sum_{<i,j>\in C} \phi(f_i, f_j, l_i, l_j) \tag{3}$$

$\lambda \geq 0$ controls the relative importance of the terms. Based on the empirical observations, λ was set to 1, giving equal weight to both terms.

ϕ is 0 if $l_i = l_j$, and otherwise $\left(1 - \exp\{-|f_i - f_j|^2/(2\sigma^2)\}\right)$, where $\sigma = \sqrt{\frac{1}{C}|f_i - f_j|}$, C is a number of clicks, and f is pixel intensity in the post-contrast image. The assignment of the labels to the pixels which minimises the energy is found with the mincut maxflow algorithm, which is known to give the global minimum [19,20].

Given the assignment of vessel / non-vessel to each voxel, we can visualise the extent of inflammation via constructing parametric maps of the heuristics and excluding the voxels corresponding to the blood vessels (Fig. 4).

4 Experiments and Discussion

An algorithm for vessel segmentation from temporal DCE-MRI slices of the MCPJs was presented. In this section, we evaluate its performance in application to 60 temporal slices.

Imaging for this application was performed on a 1.5T MRI scanner (Gyroscan ACS NT, Phillips Medical Systems, Best, The Netherlands), using a 3D T1 weighted spoiled gradient echo sequence: repetition time/echo time/flip angle = 14/3.8/40°; field of view = 100mm, slice thickness 3mm, imaging matrix is 128×256 [4].

The number of vessels seen in a slice varies from 8 to 17, and the diameter of a vessel ranges from 2 to 200 pixels. Firstly, we evaluate the algorithm's ability to detect the vessels in temporal slices by comparison of results with the ground truth (GT) provided by an experienced observer. Table 1 illustrates the results.

The algorithm did not deliver false positive results and no post-processing to remove over-segmented regions is needed. A small proportion of blood vessels of a small size (less than 5 pixels) has been classified as noise at the MRF step. However, analysing several corresponding slices, we can reconstruct the structure of the vessel tree using, for example, cubic interpolation on region locations. Fig.5 (right) illustrates the result for one of the studies. The reader gets a 'semi' 3D impression of the inflammatory distribution in the imaged area; moreover the location of under-segmented blood vessels can be recovered.

Table 1. Detection of blood vessels in temporal slices [Number of blood vessels delivered by the algorithm / Total number of vessel in the slice]; S – scan number; P – patient number

Patient / Slice	P_1	P_2	P_3	P_4	P_5	P_6	P_7	P_8	P_9	P_{10}
S_1	9/9	14/14	16/16	14/14	9/9	12/12	12/12	12/12	10/10	17/17
S_2	9/9	11/11	14/15	12/13	11/13	9/10	12/13	10/10	9/9	14/16
S_3	9/9	11/12	17/17	14/14	12/12	11/11	11/12	8/9	8/10	14/15
S_4	8/9	13/13	16/17	12/14	9/10	12/13	10/12	6/8	12/12	15/15
S_5	8/8	10/11	17/17	15/15	11/11	12/12	13/13	10/10	12/13	15/15
S_6	9/9	12/12	16/17	16/16	11/11	10/10	13/13	12/12	12/12	16/16

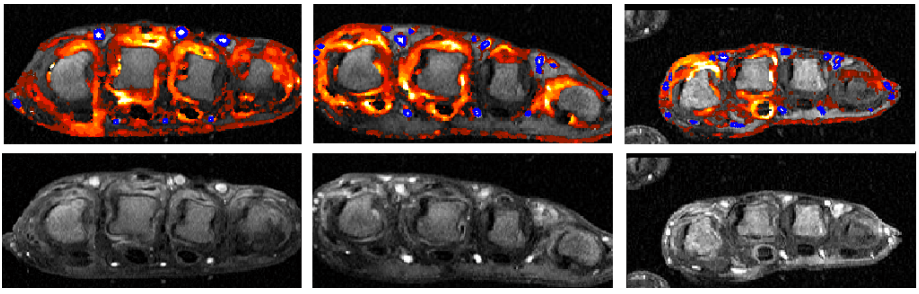

Fig. 4. Top: Parametric maps of ME corresponding to different DCE-MRI studies with segmented blood vessels (the contour is shown in blue). The lower values of the heuristic are plotted in red, then yellow and white as the values increase. Bottom: Corresponding post-contrast images.

The quality of the segmented boundaries of the vessels was evaluated using a mutual overlap based metric [21]. For 60 slices, at each step of the algorithm (PCA / PCA+EM / PCA+EM+MRF) we computed the number of erroneous voxels with respect to the overall number of voxels in the GT.

For comparison purposes we segmented BVs using the intensity of the voxels for probabilistic modelling rather than the heuristics (Alg.2 in Fig. 5).

The results obtained in this experiment indicate that the proposed algorithm generates accurate segmentation regardless of size and location of the vessels. At each step we observe an incremental increase in quality of results. On average the new algorithm detects 94% of vessels in dynamic MRI slices of the MCPJs, with mutual overlap between GT and obtained segmentations exceeding 90%.

Pixels identified as false negative are normally located around the border of segmented vessels. Their exclusion / inclusion might be due to observer misdetection and could be improved by boundary refining algorithms.

An alternative approach, where intensity of the voxels was used for probabilistic modelling rather than the heuristics (Alg.2) failed to deliver reliable segmentation – often synovial tissue was classified as vessels and vice versa.

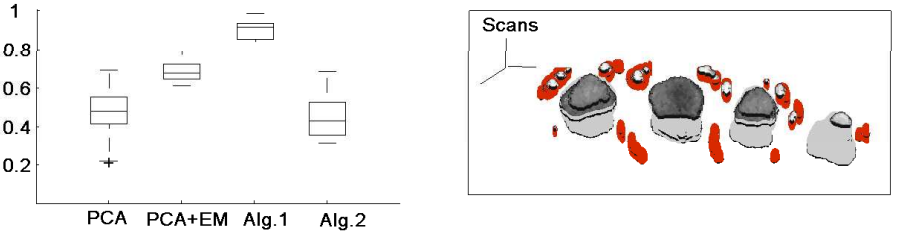

Fig. 5. Left: Mutual overlap between GT and segmented regions at each step of the proposed algorithm. Final results – Alg.1; results with an alternative segmentation technique (Alg.2). Right: Reconstructed vessels and bone interiors (3D view).

These results confirm that voxel intensity based modelling alone is not sufficient for accurate tissue classification.

5 Conclusion

The method presented in this paper delivers accurate segmentation of blood vessels from DCE-MRI datasets of the hand joints. Statistical mixture models motivated by the physiological properties of the individual tissues, such as speed of absorption and concentration of the contrast agent, have been employed to describe the behaviour of the vessels and synovitis. Spatial relationships between neighbouring pixels were incorporated through an MRF probabilistic framework. The combination of these methods provides promising results. The technique is fully automated, does not require any post-processing and can easily be adapted for other applications of the similar nature. Future work will focus on the testing of the method on datasets acquired from different joints and investigation of the algorithm's performance when other heuristics are included.

References

1. Taylor, P.C.: The value of sensitive imaging modalities in rheumatoid arthritis. Arthritis Research and Therapy 5(5), 210–213 (2003)
2. McQueen, F.M., Stewart, N., Crabbe, J., Robinson, E., Yeoman, S., Tan, P.L.J., McClean, L.: Magnetic resonance imaging of the wrist in early rheumatoid arthritis reveals a high prevalence of erosion at four months after symptom onset. Annals of the Rheumatic Diseases 57, 350–356 (1998)
3. Cimmino, M.A., Innocenti, S., Livrone, F., Magnaguagno, F., Silvesti, E., Garlaschi, G.: Dynamic gadolinium-enhanced MRI of the wrist in patients with rheumatoid arthritis. Arthritis and Rheumatism 48(5), 674–680 (2003)
4. Radjenovic, A.: Measurement of physiological variables by dynamic Gd-DTPA enhanced MRI. PhD thesis, School of Medicine, University of Leeds (2003)
5. Jackson, A.: Analysis of dynamic contrast enhanced MRI. Radiology 77(2), 154–166 (2004)
6. Kubassova, O., Boyle, R.D., Radjenovic, A.: Improved parameter extraction from dynamic contrast-enhanced MRI data in RA studies. In: Joint Disease Workshop, Medical Image Computing and Computer Assisted Intervention, vol. 1, pp. 64–71 (2006)
7. Kirbas, C., Quek, F.: A review of vessel extraction techniques and algorithms. ACM Computing Surveys 36(2), 81–121 (2004)
8. Suri, J.S., Liu, K., Reden, L., Laxminarayan, S.: A review on MR vascular image processing algorithms: acquisition and prefiltering: Part I. IEEE Transactions on Information Technology in Biomedicine 6(4), 324–337 (2002)
9. Sonka, M., Liang, W., Stefancik, R.M., Stolpen, A.: Vascular Imaging and Analysis. In: Sonka, M., Fitzpatrick, J.M. (eds.) Handbook of Medical Imaging. Medical Image Processing and Analysis, SPIE, pp. 808–914 (2000)
10. Bulpitt, A., Berry, E., Boyle, R., Scott, J., Kessel, D.A.: A deformable model, incorporating expected structure information, for automatic 3D segmentation of complex anatomical structures. Computer Assisted Radiology and Surgery 1, 572–577 (2000)

11. Magee, D., Bulpitt, A., Berry, E.: 3D automated segmentation and structural analysis of vascular trees using deformable models. IEEE Workshop on Variational and Level Set Methods in Computer Vision 1, 119–126 (2001)
12. McInerney, T., Terzopoulos, D.: Deformable models in medical image analysis: a survey. Medical Image Analysis 1(2), 91–108 (1996)
13. Tofts, P.S., Kermode, A.G.: Measurement of the blood-brain barrier permeability and leakage space using DEMRI. Magnetic Resonance in Medicine 17(2), 357–367 (1991)
14. Chung, A.C.S., Noble, J.A., Summers, P.: Vascular segmentation of phase contrast magnetic resonance angiograms based on statistical mixture modeling and local phase coherence. IEEE Transactions on Medical Imaging 23(12), 1490–1507 (2004)
15. Wilson, D.L., Noble, J.A.: An adaptive segmentation algorithm for time-of-flight MRA data. Medical Imaging 18, 938–945 (1999)
16. Klarlund, M., Øsrergaard, M., Rostrup, E., Skødt, H., Lorenzen, I.: Dynamic MRI and principal component analysis of finger joints in rheumatoid arthritis, polyarthritis, and healthy controls. International Society for MRI in Medicine (last access on 03.05.07) (1999), http://cds.ismrm.org/ismrm-1999/PDF2/409.pdf
17. Ridler, T.W., Calvard, S.: Picture thresholding using an iterative selection method. Man and Cybernetics 8(8), 630–632 (1978)
18. Geman, S., Geman, D.: Stochastic relaxation, Gibbs distributions, and the Bayesian restoration of images. IEEE Transactions on Pattern Analysis and Machine Intelligence 6, 721–741 (1984)
19. Boykov, Y., Lee, V.S., Rusinek, H., Bansal, R.: Segmentation of dynamic N-D data sets via graph cuts using Markov models. In: Niessen, W.J., Viergever, M.A. (eds.) MICCAI 2001. LNCS, vol. 2208, pp. 1058–1066. Springer, Heidelberg (2001)
20. Szeliski, R., Zabih, R., Scharstein, D., Veksler, O., Kolmogorov, V., Agarwala, A., Tappen, M., Rother, C.: Comparative study of energy minimization methods for markov random fields. European Conference on Computer Vision 2, 16–29 (2006)
21. Dice, L.R.: Measures of the amount of ecologic association between species. Ecology 26(3), 297–302 (1945)